Journal of Chemistry and Technologies, 2025, *33*(4), 1026-1044

Journal of Chemistry and Technologies

pISSN 2663-2934 (Print), ISSN 2663-2942 (Online).

journal homepage: http://chemistry.dnu.dp.ua
editorial e-mail: chem.dnu@gmail.com

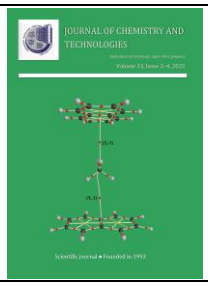

UDC 544.65

ELECTRODEPOSITION OF Ni-BASED COMPOSITE COATINGS CONTAINING CERIUM COMPOUNDS FROM A DEEP EUTECTIC SOLVENT AND THEIR ELECTROCATALYTIC PERFORMANCE

Vyacheslav S. Protsenko[1*], Denys A. Shaiderov[1], Oleksandr D. Sukhatskyi[1], Sergiy A. Korniy[1,2]
[1]*Ukrainian State University of Science and Technologies, Lazaryan Str. 2, Dnipro, 49010, Ukraine*
[2]*Karpenko Physico-Mechanical Institute of the NAS of Ukraine, Naukova Str. 5, Lviv, 79060, Ukraine*
Received 11 August 2025; accepted 2 September 2025; available online 25 December 2025

Abstract

This work examines the electrodeposition of Ni-based composite coatings containing cerium compounds from a eutectic mixture of choline chloride and urea (reline), a typical deep eutectic solvent. The data reveal that depending on the concentrations of $NiCl_2{\cdot}6H_2O$ and $CeCl_3{\cdot}7H_2O$ dissolved in reline, coatings containing up to 49 wt.% cerium, present as embedded CeO_2, can be formed within an electrochemically deposited nanocrystalline nickel matrix. Variation of the Ni(II) and Ce(III) salt concentrations strongly influences the resulting surface morphology. Reaction schemes for the formation of these composite coatings are proposed, and cyclic voltammetry with successive scan cycles was used to identify the potential windows in which the relevant electrochemical reactions occur in reline-based solutions. The deposited coatings were tested as electrocatalysts for water electrolysis in 1 M NaOH. Special attention was paid to the electrocatalytic activity of the Ni-based composite coatings toward the anodic oxidation of urea, a potential alternative to the oxygen evolution reaction in green hydrogen production. Incorporation of CeO_2 into the nickel matrix led to a pronounced enhancement of electrocatalytic activity for hydrogen evolution, oxygen evolution and urea oxidation in alkaline aqueous solution. The proposed composite coatings may find application as multifunctional catalysts for green hydrogen generation. Moreover, adjusting the Ni(II) and Ce(III) concentrations in the deep eutectic solvent-based plating bath enables flexible and controlled tuning of the electrocatalytic behavior of deposited coatings.

Keywords: electrodeposition; nickel; ceria; deep eutectic solvent; composite coating; green hydrogen production; urea oxidation reaction; electrocatalysis.

ЕЛЕКТРООСАДЖЕННЯ КОМПОЗИЦІЙНИХ ПОКРИТТІВ НА ОСНОВІ НІКЕЛЮ, ЩО МІСТЯТЬ СПОЛУКИ ЦЕРІЮ, З НИЗЬКОТЕМПЕРАТУРНОГО ЕВТЕКТИЧНОГО РОЗЧИННИКА ТА ЇХ ЕЛЕКТРОКАТАЛІТИЧНА АКТИВНІСТЬ

Вячеслав С. Проценко[1*], Денис А. Шайдеров[1], Олександр Д. Сухацький[1], Сергій А. Корній[1,2]
[1]*Український державний університет науки і технологій, вул. Лазаряна, 2, м. Дніпро, 49010, Україна*
[2]*Фізико-механічний інститут ім. Карпенка НАН України, вул. Наукова, 5, м. Львів, 79060, Україна*

Анотація

Дана робота розглядає основні патерни електроосадження композиційних покриттів на основі нікелю, що містять сполуки церію, отриманих з розчину на основі евтектичної суміші холін хлориду і сечовини (розчинник reline), який є типовим представником нового покоління іонних рідин – deep eutectic solvents. Отримані дані показують, що в залежності від концентрації розчинених в reline солей $NiCl_2{\cdot}6H_2O$ і $CeCl_3{\cdot}7H_2O$ на катоді можливе формування покриттів, що містять до 49 % церію у формі діоксиду, що впроваджений у електрохімічно осаджену нанокристалічні нікелеву матрицю. Варіювання концентраціями солей нікелю(II) і церію(III) суттєво впливає на характер морфології поверхні. Запропоновано реакційні схеми утворення композиційного покритті та методом циклічної вольтамперометрії з послідовними сканами циклювання визначено інтервали потенціалів проходження електрохімічних реакцій у розчинах на основі reline. Осаджені покриття тестовано як потенційні електрокаталізатори у електродних процесах при електролізі води (1 M NaOH). Особлива увага приділена електрокаталітичній активності осаджених композиційних покриттів на основі нікелю у реакції анодного окислення карбаміду, що є потенційною альтернативою анодному виділенню кисню при синтезі зеленого водню. Показано помітне зростання електрокаталітичної активності при впровадженні діоксиду церію до нікелевої матриці в процесах виділення водню, кисню та анодного окислення карбаміду в водному лужному розчині. Запропоновані електрокаталітичні покриття можуть знайти застосування як поліфункціональні каталізатори для генерації зеленого водню в водневій енергетиці. Варіювання концентраціями солі нікелю(II) і церію(III) у ванні осадження на основі DES дозволяє проводити гнучкий і керований тюнинг електрокаталітичної поведінки отримуваних покриттів.

Ключові слова: електроосадження; нікель; церій оксид; низькотемпературний евтектичний розчинник; композиційне покриття; продукування зеленого водню; електроокислення карбаміду; електрокаталіз.

**Corresponding author: e-mail: vprotsenko7@gmail.com*
 doi: 10.15421/jchemtech.v33i4.337132

Journal of Chemistry and Technologies, 2025, *33*(4), 1026-1044

Introduction

The global shift toward the development and deployment of integrated technologies for green hydrogen energy, among other goals, demands the creation of new, highly efficient, readily available, and low-cost electrochemical systems for electrolytic hydrogen production and the corresponding electrocatalysts [1–4]. Among the various alternatives currently examined in the literature for hydrogen-generating electrolysis, particular attention has been paid to a system in which the cathodic hydrogen evolution reaction in an alkaline medium (reaction (1)) is coupled with the anodic urea oxidation reaction (reaction (2)) [5–8].

$$2H_2O + 2e^- \rightarrow H_2 + 2OH^- \quad (1)$$

$$CO(NH_2)_2(aq) + 8OH^- \rightarrow N_2(g) + 6H_2O + CO_3^{2-}(aq) + 6e^- \quad (2)$$

Thus, in such an electrochemical system, the "traditional" oxygen evolution reaction at the anode (reaction (3)) is replaced by the urea oxidation reaction (reaction (2)), which is characterized by a lower thermodynamic potential [6–10].

$$4OH^- \rightarrow O_2 + 2H_2O + 4e^- \quad (3)$$

As a result of this substitution, the anodic potential is significantly lowered, thereby reducing both the overall cell voltage of the electrolyzer and its total energy consumption during electrolysis.

However, a major challenge in deploying such electrochemical systems for green hydrogen generation is the still insufficient electrocatalytic activity of existing electrode materials, particularly those used in the anodic urea oxidation process (2) [6; 7; 11–13]. Hence, the development of new, readily available, low-cost, and highly efficient electrocatalysts for the urea oxidation reaction is imperative.

Among the various research directions aimed at addressing this challenge, electrochemical deposition of coatings based on nickel and other transition metals appears especially promising [6; 7; 14; 15]. Advantages of synthesizing electrocatalysts by electrodeposition technique include the ability to precisely control the thickness as well as the chemical and phase compositions of the deposited layers by varying deposition time, applied potential, current density, and electrolyte composition [16]. Other benefits include typically high coating adhesion to the substrate, operational simplicity, wide accessibility, and relatively low equipment cost. For example, the literature reports nanostructured electroplated NiMoSe films [17] and $CeNi_2$@NiO composites [18] that have demonstrated high electrocatalytic performance for hydrogen evolution coupled with urea oxidation.

Further development and enhancement of electrodeposited electrocatalytic materials for hydrogen energy can be achieved, among other approaches, by moving to new electrolytic deposition systems, in particular those based on deep eutectic solvents (DESs) [19–21]. DESs are a special class of low-temperature ionic liquids formed by mixing various organic and/or inorganic components in eutectic or near-eutectic proportions [22–24]. Owing to their unique set of properties, DESs are now regarded as highly promising solvents for the synthesis of novel, high-performance electrocatalysts for hydrogen energy, especially via electrochemical deposition [19; 21; 25–27].

In our previous studies, we demonstrated the feasibility of electrodepositing nickel-based coatings from DES-based solutions [28] and confirmed their high electrocatalytic activity for hydrogen evolution [29] and oxygen evolution [30]. We also found that the incorporation of *in situ* formed CeO_2 particles into the nickel matrix electrodeposited from a DES-based electrolyte yields a composite coating with enhanced functional properties, in particular increased catalytic activity for hydrogen evolution [31] and for the anodic oxidation of urea in alkaline media [32]. However, a number of important questions remain unanswered regarding the characteristics of composite electrodeposition from DES-based electrolytes and their electrocatalytic behavior. In particular, the influence of the concentrations of electrolyte components, dissolved Ni(II) and Ce(III) salts, on the chemical composition and electrocatalytic properties of the resulting coatings has not been characterized, although this is critical for developing high-performance electrocatalytic materials. The reaction pathway leading to the formation of Ni-based composite coatings containing cerium compounds has not been elucidated, nor have the details of the electrochemical kinetics of the associated processes been clarified. The effect of Ni and Ce salt concentrations in DES on the electrocatalytic activity of the coatings toward urea oxidation also remains unknown. The present work is devoted to addressing these issues.

Journal of Chemistry and Technologies, 2025, *33*(4), 1026-1044

Experimental

The deep eutectic solvent (reline) was prepared by mixing calculated and weighed amounts of choline chloride and urea in a 1 : 2 molar ratio. Commercial choline chloride $[(CH_3)_3NCH_2CH_2OH]Cl$ (99 %, Acros Organics; CAS 67-48-1) and urea $CO(NH_2)_2$ (99.9 %, Nile Chemicals; CAS 57-13-6) were used without further purification. The mixture was stirred on a magnetic stirrer at approximately 70 °C for several hours until a clear, homogeneous liquid formed.

Nickel(II) chloride hexahydrate $NiCl_2{\cdot}6H_2O$ (>99 %, Sigma-Aldrich; CAS 7791-20-0) and cerium(III) chloride heptahydrate $CeCl_3{\cdot}7H_2O$ (99.9 %, Suzhou Leba Chemical Co., Ltd; CAS 18618-55-8) were used as sources of Ni^{2+} and Ce^{3+} ions. Calculated and accurately weighed amounts of these salts were added to the measured volume of reline and stirred on a magnetic stirrer at 70 °C until complete dissolution.

Electrodeposition of the coatings was carried out on degreased copper foil substrates with a surface area of 1 cm^2. A galvanostatic deposition mode was employed using a stabilized DC power supply (Electronics 30 V 6 A) in a thermostatted glass cell. A nickel plate served as the anode. The electrolyte volume in the cell was 100 mL. Deposition was performed at a cathodic current density of 3 mA/cm^2 and a temperature of 70±0.01 °C under constant magnetic stirring at approximately 500 rpm. The deposition time was 60 minutes.

All voltammetric measurements were performed with a Reference 3000 potentiostat (Gamry). Cyclic voltammograms in reline-based electrolytes were recorded in a three-electrode glass cell thermostatted at 70±0.01 °C. The working electrode was a platinum disc sealed in glass, the counter electrode was a nickel plate, and a silver wire immersed in the DES served as a quasi-reference electrode. Experiments employed successive scan cycles (11 consecutive cycles). Each measurement began from the experimentally determined open-circuit potential (OCP) and proceeded first in the cathodic direction, then reversed anodically, and finally returned cathodically. The potential scan rate was 100 mV/s.

Electrocatalytic activity was evaluated by cyclic voltammetry at a scan rate of 50 mV/s in aqueous solutions of 1 M NaOH or 1 M NaOH + 0.33 M $CO(NH_2)_2$. These solutions were prepared by dissolving the requisite amounts of sodium hydroxide (analytical grade; CAS 1310-73-2) and urea in distilled water. The electrochemical cell was thermostatted at 25±0.01 °C, and dissolved oxygen was removed by bubbling purified hydrogen through the solution. The working electrode was the deposited coating on a copper substrate held in a plastic cassette. A platinum wire served as the counter electrode, and a saturated silver–silver chloride electrode was used as the reference. All potentials were converted to the standard hydrogen electrode scale. The cell's ohmic drop was measured and automatically compensated by the built-in potentiostat compensation circuit.

The surface morphology of the electrodeposited coatings was examined using a scanning electron microscope (SEM, Zeiss EVO 40XVP). The chemical composition of the coating surfaces was determined by energy-dispersive X-ray spectroscopy (EDX) with an Oxford INCA Energy 350 attachment integrated into the microscope. Phase composition analysis was carried out using a DRON-2 X-ray diffractometer with monochromatized Co-K_α radiation (λ = 1.7902 Å).

Results and discussion

Based on preliminary experiments, it was established that compact coatings with satisfactory adhesion to the substrate can be obtained in the studied system at nickel salt ($NiCl_2{\cdot}6H_2O$) concentrations of 0.2 and 0.3 mol/dm^3 in reline. The concentration of dissolved cerium salt ($CeCl_3{\cdot}7H_2O$) was varied at 0; 0.1; 0.2; 0.3; 0.4; and 0.5 mol/dm^3. Table 1 presents the chemical composition of the coatings deposited from electrolytes with the specified concentrations of nickel and cerium salts, as determined by EDX analysis. Corresponding SEM surface images are shown in Figure 1.

The chemical composition of the coatings revealed the presence of elements such as nickel, cerium, oxygen, carbon, and nitrogen (in some samples). The presence of nickel is evidently attributed to the electrodeposition process. A number of other electrochemical and chemical transformations occurring in the near-electrode region (see discussion below) are apparently responsible for the incorporation of cerium and oxygen into the coatings. The main pathway for the inclusion of carbon and nitrogen in the deposited material is likely the adsorption and occlusion of organic electrolyte components and/or the products of their chemical and

Journal of Chemistry and Technologies, 2025, *33*(4), 1026-1044

electrochemical degradation during the growth of the coating.

Table 1

Chemical composition of the deposited coatings according to EDX analysis

Concentration of Ni(II) ions in the electrolyte, mol/dm³	Concentration of Ce(III) ions in the electrolyte, mol/dm³	Elemental composition of the coating, wt.%				
		Ni	Ce	C	O	N
0.2	–	86.44	–	7.94	5.62	–
	0.1	88.46	0.36	7.81	3.37	–
	0.2	91.90	1.11	4.54	2.45	–
	0.3	84.17	6.79	5.39	3.65	–
	0.4	76.86	12.88	5.79	4.47	–
	0.5	56.51	28.39	6.40	8.70	–
0.3	–	91.52	–	6.46	2.02	–
	0.1	79.77	2.75	9.95	7.53	–
	0.2	66.98	5.71	11.16	14.79	1.36
	0.3	66.05	7.09	12.01	13.58	1.27
	0.4	32.95	41.92	7.63	15.99	1.51
	0.5	24.44	49.41	6.83	17.45	1.87

With increasing Ce(III) ion concentration in the electrolyte, a corresponding increase in the cerium content in the deposited layer is observed, while the nickel content decreases. At low Ce(III) concentrations (0.1 mol/dm³), the main component of the coating is nickel, and the mass fraction of cerium remains at trace levels, comparable to the detection limit of the EDX method. As the Ce(III) ion concentration increases, the cerium content in the coating rises significantly, and at concentrations of 0.3 mol/dm³ Ni(II) and 0.5 mol/dm³ Ce(III), cerium becomes the predominant component in the deposited layer. A simultaneous increase in oxygen content is also observed with the rise in cerium content. The carbon content in the coatings ranges from approximately 5 to 12 wt.%, with no clear correlation to the concentrations of Ni(II) and Ce(III) salts.

Interestingly, under equal concentrations of Ce(III) ions in the solution, an increase in the Ni(II) ion concentration from 0.2 to 0.3 mol/dm³ leads not to an increase, as might be expected, but to a decrease in the nickel content in the coatings, while the cerium content in the deposited layer simultaneously increases.

SEM images (Fig. 1) reveal a gradual transformation in the surface topography of the electrodeposited coatings with increasing concentrations of $NiCl_2 \cdot 6H_2O$ and $CeCl_3 \cdot 7H_2O$ in the reline-based solution. In the absence of cerium ions in the deposition bath, the coating surface exhibits a compact spheroidal structure without noticeable surface relief defects. At a Ni(II) concentration of 0.2 mol/dm³, the size of the nickel spheroids on the surface is slightly larger than that observed at 0.3 mol/dm³ Ni(II).

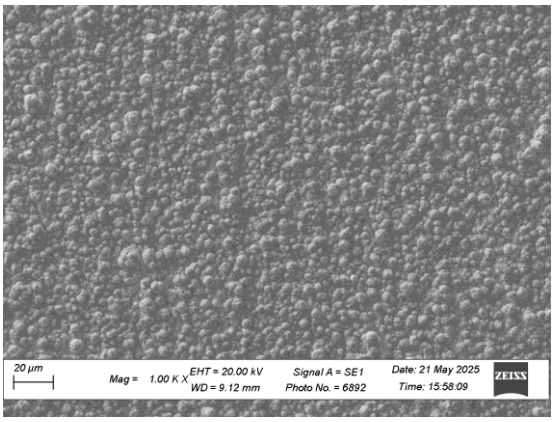

a

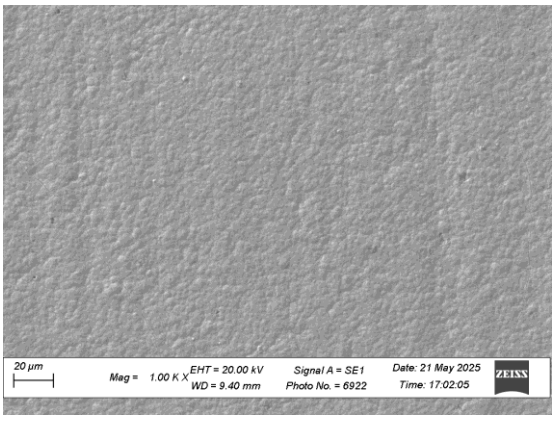

g

Journal of Chemistry and Technologies, 2025, *33*(4), 1026-1044

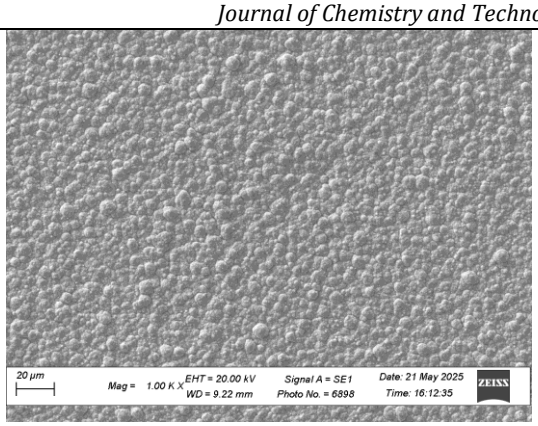

b

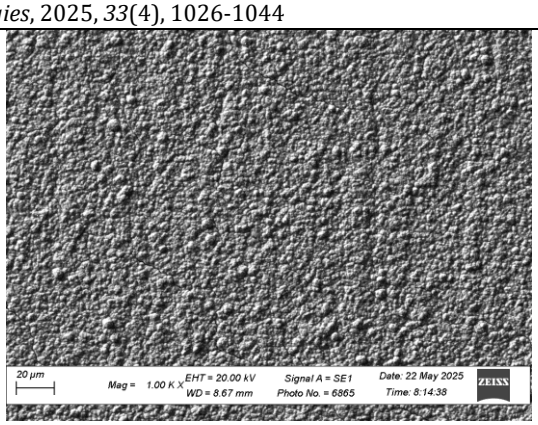

h

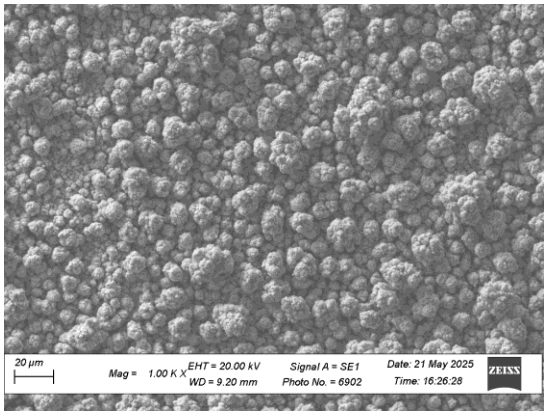

c

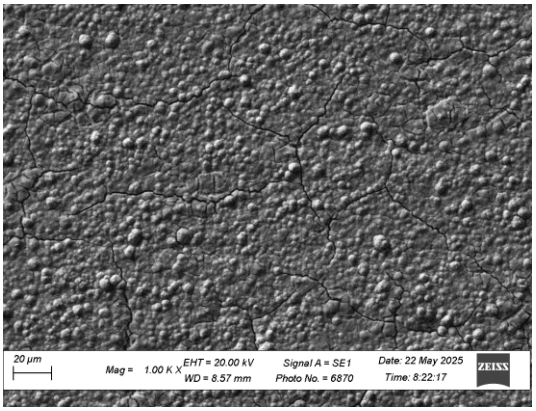

i

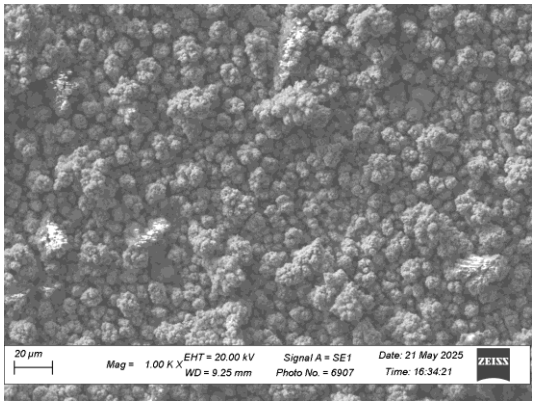

d

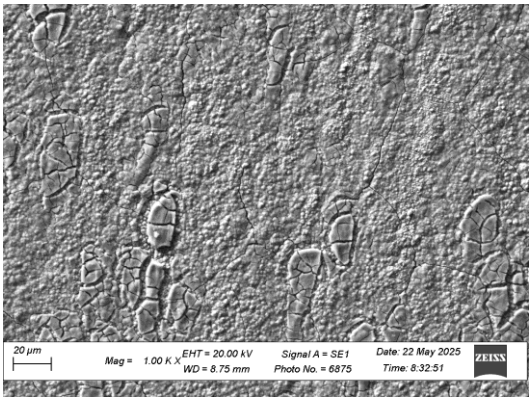

j

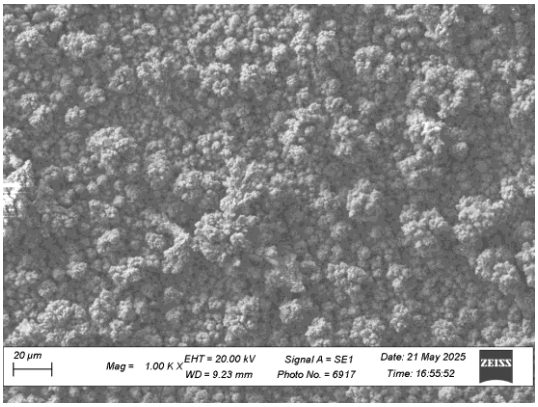

e

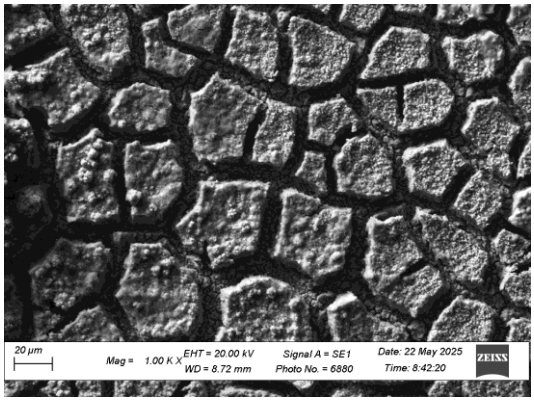

k

Journal of Chemistry and Technologies, 2025, *33*(4), 1026-1044

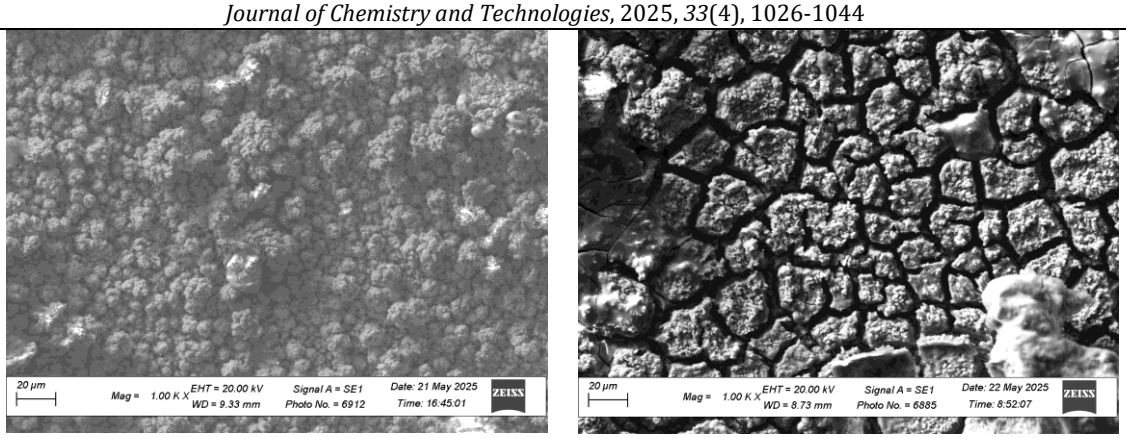

f **l**

Fig. 1. SEM images of the surface of coatings deposited from reline-based electrolytes containing 0.2 mol/dm³ $NiCl_2 \cdot 6H_2O$ (left column – a, b, c, d, e, and f) and 0.3 mol/dm³ $NiCl_2 \cdot 6H_2O$ (right column – g, h, i, j, k, and l) with varying concentrations of $CeCl_3 \cdot 7H_2O$ salt (mol/dm³): a and g – 0; b and h – 0.1; c and i – 0.2; d and j – 0.3; e and k – 0.4; and f and l – 0.5

The introduction of 0.1 mol/dm³ $CeCl_3 \cdot 7H_2O$ into the electrolyte containing 0.2 mol/dm³ $NiCl_2 \cdot 6H_2O$ has almost no effect on the surface morphology (Fig. 1a and b), likely due to the fact that the chemical composition of the coating remains practically unchanged under these conditions (Table 1), and the incorporation of cerium (or its compounds) is negligible. In contrast, the addition of 0.1 mol/dm³ $CeCl_3 \cdot 7H_2O$ to the DES-based electrolyte containing 0.3 mol/dm³ $NiCl_2 \cdot 6H_2O$ results in the formation of numerous prominently protruding asymmetric crystallites on the surface.

With further increase in cerium ion concentration (0.2 mol/dm³ and higher), SEM images of samples deposited from the electrolyte containing 0.2 mol/dm³ $NiCl_2 \cdot 6H_2O$ reveal the formation of characteristic agglomerates resembling cauliflower morphology, which create numerous protrusions and depressions on the surface. The surface morphology of Ni–Ce-containing samples deposited from the electrolyte with a higher nickel salt concentration (0.3 mol/dm³ $NiCl_2 \cdot 6H_2O$) is notably different: at cerium ion concentrations of 0.2 and 0.3 mol/dm³ $CeCl_3 \cdot 7H_2O$, surface defects appear (microcracks and large asymmetric crystallites protruding from the surface), while at 0.4 and 0.5 mol/dm³ $CeCl_3 \cdot 7H_2O$, the surface consists of asymmetric flake-like islands with sizes of about 20–30 μm, separated by wide cracks 5–10 μm in width. As a general trend, the incorporation of cerium-containing compounds leads to a significant increase in surface defectiveness and geometrical heterogeneity of the coatings, which is, in principle, favorable for enhancing the activity of electrocatalysts.

The microstructural investigation of the coatings by X-ray diffraction revealed that nanocrystalline coatings with a nanocrystalline face-centered cubic (fcc) Ni lattice are formed from reline-based electrolytes. This is evidenced by the broadened diffraction peaks at 2θ = 52.5°, 61.4°, 92.4°, 115.3°, and 124.2° (Fig. 2a), which correspond to the (111), (200), (220), (311), and (222) crystal planes, respectively. The average crystallite size, estimated using the Scherrer equation, is approximately 30–60 nm. It is worth noting that the formation of nanocrystalline nickel during electrodeposition from DES-based electrolytes has been frequently reported in the literature [29; 31; 33; 34], and is attributed to the inhibition of nucleation and growth stages due to strong adsorption of organic components of the electrolyte on the growing nickel layer.

Journal of Chemistry and Technologies, 2025, *33*(4), 1026-1044

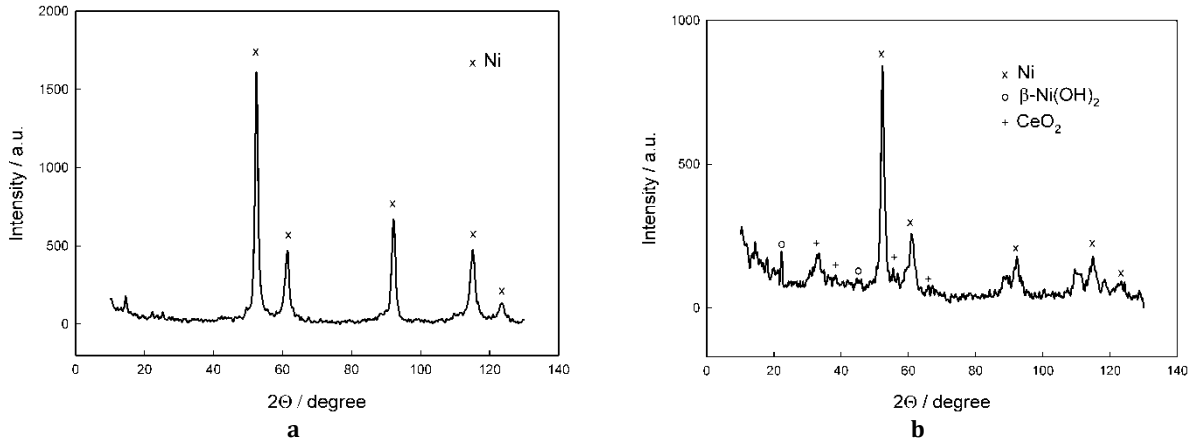

Fig. 2. Typical XRD patterns of the coatings electrodeposited from reline-based electrolytes containing 0.3 mol/dm³ $NiCl_2 \cdot 6H_2O$ (a) and 0.3 mol/dm³ $NiCl_2 \cdot 6H_2O$ + 0.3 mol/dm³ $CeCl_3 \cdot 7H_2O$ (b)

The X-ray diffraction pattern of the sample obtained from the electrolyte containing both nickel and cerium salts (Fig. 2b) shows, in addition to the reflections of the nanocrystalline α-Ni phase, weak peaks corresponding to nickel hydroxide β-$Ni(OH)_2$ (2θ = 22.4° and 45.1°, corresponding to the (001) and (101) crystal planes, respectively) and cerium dioxide CeO_2 (2θ = 32.5°, 38.3°, 55.1°, and 65.7°, originating from the (111), (200), (220), and (311) planes, respectively). Despite the relatively high cerium content in the coating (as indicated by EDX analysis), the diffraction peaks of the CeO_2 phase are of low intensity and somewhat broadened, likely due to its high degree of hydration and the presence of cerium in an X-ray amorphous state. No diffraction maxima corresponding to metallic cerium or its intermetallic compounds with nickel were observed.

Thus, based on a comprehensive analysis of the above experimental results and literature data, the following reaction scheme can be proposed for the processes occurring during the formation of the investigated coatings. The main electrochemical process at the cathode is evidently the electrodeposition of nanocrystalline nickel, which proceeds according to the following reaction:

$$Ni(II) + 2e^- \rightarrow Ni \quad (4)$$

In addition to this reaction, the discharge of water molecules also occurs at the cathode in the DES-based electrolyte [35], with the main source of water being the crystallization water from the $NiCl_2 \cdot 6H_2O$ and $CeCl_3 \cdot 7H_2O$ crystalline hydrates dissolved in reline:

$$2H_2O + 2e^- \rightarrow H_2 + OH^- \quad (5)$$

As a result of the local accumulation of hydroxide ions in the near-electrode layer, the formation of a certain amount of nickel hydroxide becomes possible, which is incorporated into the deposited film via the following reaction [36]:

$$Ni^{2+} + 2OH^- \rightarrow Ni(OH)_2 \quad (6)$$

Nickel hydroxide incorporated into the coating, in particular, plays an important role in enhancing its electrocatalytic activity [29].

Furthermore, the local increase in OH^- ion concentration promotes the formation of dispersed cerium(IV) dioxide particles via a mechanism similar to that described in several previous studies [37–39]. In particular, chemical reactions leading to the formation of CeO_2 may occur in the near-electrode layer and directly on the cathode surface according to the following reactions [40; 41]:

$$Ce^{3+} + 3OH^- \rightarrow Ce(OH)_3 \quad (7)$$

$$4Ce^{3+} + O_2 + 4OH^- + 2H_2O \rightarrow 4[Ce(OH)_2]^{2+} \quad (8)$$

$$4Ce(OH)_3 + O_2 \rightarrow 4CeO_2 + 6H_2O \quad (9)$$

$$[Ce(OH)_2]^{2+} \rightarrow CeO_2 + 2H^+ \quad (10)$$

The oxidizing agent converting Ce(III) to Ce(IV) in this system is oxygen, which can dissolve in reline upon contact with air and subsequently participate in chemical transformations [42]. It is important to note that in the course of reactions (5) and (8), water is consumed, the source of which in this ionic liquid environment is the crystallization water introduced along with the $NiCl_2 \cdot 6H_2O$ and $CeCl_3 \cdot 7H_2O$ salts. In this context, it should be

Journal of Chemistry and Technologies, 2025, *33*(4), 1026-1044

emphasized that an increase in the concentration of nickel and cerium ions automatically implies a corresponding increase in the water content in the solution, thereby accelerating the *in situ* formation of dispersed cerium dioxide particles according to the reaction scheme (7–10), which are subsequently incorporated into the coating. We suggest that this effect is particularly related to the observed increase in CeO_2 content in the coating not only with increasing $CeCl_3 \cdot 7H_2O$ concentration (which is expected), but also with increasing $NiCl_2 \cdot 6H_2O$ concentration in the electrolyte (which, in principle, is a non-trivial result as noted above in Table 1).

As can be seen from the data presented in Table 1, the measured Ce:O mass ratio is substantially lower than the stoichiometric value for CeO_2 (experimental values derived from EDX spectra range from 0.11 to 3.26, whereas the theoretical value for CeO_2 is 4.375). This deviation can be explained by oxygen associated with nickel-containing phases present in the deposit (e.g., $Ni(OH)_2$) and with other oxygen-bearing compounds (such as adsorbed or occluded organic molecules and water), rather than being exclusively bound to cerium dioxide. In other words, the apparent deficit of Ce relative to O mainly reflects oxygen not bonded to cerium, together with the inherent uncertainties of EDX quantification for light elements. It should be emphasized that the absence of hydrogen detection in EDX affects only the normalization to 100 % and does not alter the Ce:O ratio itself.

In the DES environment, in the near-cathode region, transformation of the choline cation may also occur via the Hoffmann elimination reaction, resulting in the formation of trimethylamine [43]:

$$\left[(CH_3)_3\overset{+}{N}-CH_2-CH_2-OH\right]+OH^- \rightarrow N(CH_3)_3+CH_2=CH-OH+H_2O \quad (11)$$
$$\Updownarrow$$
$$CH_3-CH=O$$

The choline cation may also participate in direct electrochemical transformations at the cathode, forming a choline radical that subsequently can be converted either into trimethylamine and an ethanol radical or into dimethylaminoethanol and a methyl radical [43]. The organic components of the electrolyte, as well as the aforementioned products of their chemical and electrochemical transformations, can adsorb onto the surface of the deposited nickel matrix, nickel hydroxide, and cerium dioxide, thereby becoming incorporated into the coating. This explains the presence of metalloids such as carbon, nitrogen, and oxygen in the deposit (Table 1).

To detail the proposed reaction mechanism of composite nickel-cerium coating formation and to elucidate the kinetics of the corresponding electrochemical reactions, cyclic voltammograms (CVs) were recorded in solutions of nickel and cerium salts in reline (Figures 3–6). Since electrochemical processes occurring under potential scan conditions can induce changes both in the electrode surface state and in the composition of the electrolyte near the electrode, the method of cyclic voltammetry with multiple consecutive scan cycles was employed.

The cyclic voltammogram of a platinum electrode in reline (Fig. 3) exhibits a typical shape previously reported in the literature [44]: during the initial cathodic scan, an intense exponential current increase is observed at potentials more negative than –0.7 V, associated with the cathodic decomposition of the solvent (negative limit of the solvent's "electrochemical window"). Additionally, a small wave appears at approximately –0.6 V on the cathodic scan, likely related to the reduction of urea molecules adsorbed on the platinum surface [44]. On the anodic scan, a distinct current wave appears near –0.8 V due to the partial reduction of oxidation products of organic components formed during the preceding anodic scan. A relatively broad anodic current wave in the potential range 0–1 V can be attributed to the electrochemical oxidation of certain components of the eutectic solvent, particularly urea. Finally, the increase in anodic current beyond approximately 1.2 V corresponds to reaching the positive limit of the electrochemical window of the eutectic solvent; according to ref. [43], the current in this potential region is related to the formation of the Cl_3^- ion, which rapidly reacts with DES components, producing various chlorinated products. Importantly, the cyclic voltammograms recorded during the first 11 cycles practically coincide, indicating the absence of significant surface state evolution of the platinum electrode under these conditions and confirming a quasi-stationary regime.

Journal of Chemistry and Technologies, 2025, *33*(4), 1026-1044

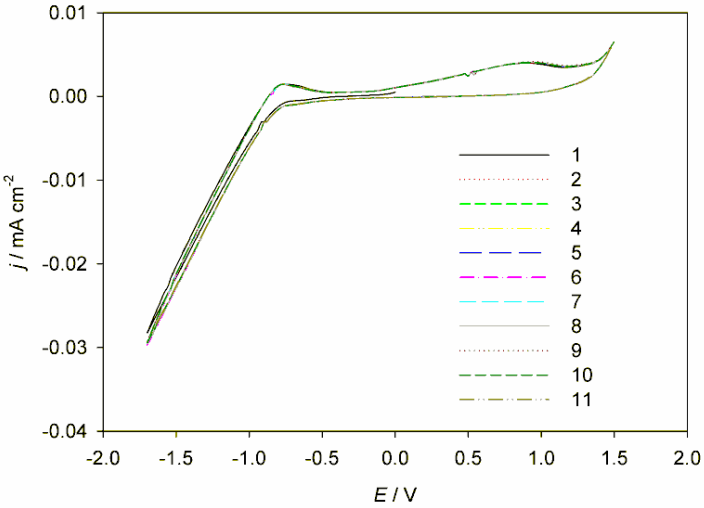

Fig. 3. Cyclic voltammograms of a platinum electrode in reline during consecutive multiple potential scans (100 mV/s, 70 °C). The numbers indicate the sequence of scan cycles

The CVs recorded in a solution containing 0.2 M Ce(III) in reline (Fig. 4), in addition to the characteristic regions described above, display cathodic current waves at potentials of –0.6…–0.8 V and anodic current waves at –0.5…–0.4 V. Interestingly, in the first few potential scans these waves are only weakly pronounced and become clearly visible on the CVs only after a certain number of scanning cycles, with the reproducibility of these data in parallel experiments being rather unsatisfactory. Considering these facts, we assume that during potential sweeping at the Pt electrode, CeO_2 (most likely in a colloidal state) is formed on the anodic scan as a result of Ce(III) ion oxidation (the indicated anodic wave at –0.5…–0.4 V), leading to the accumulation of CeO_2 dispersion in the near-electrode layer of the electrolyte and directly on the electrode surface. This CeO_2 can then be electrochemically reduced (at the mentioned cathodic wave at –0.6…–0.8 V). These electrode processes can be represented for the anodic direction of their occurrence by the following reaction scheme:

$$Ce^{3+} + 2H_2O \Leftrightarrow CeO_2 + 4H^+ + e^- \qquad (12)$$

It is evident that the oxidation products of Ce(III) in the form of a colloidal dispersion can partially diffuse away from the electrode surface into the bulk of the solution, accumulating there without being fully reduced during the cathodic scan. Interestingly, this assumption is supported by visual observations concerning the chemical instability of cerium(III) salt solutions in reline during prolonged storage in contact with air. These observations revealed that such electrolytes become turbid after several weeks due to the gradual accumulation of colloidal cerium dioxide as a result of reactions (7–10). At high concentrations of cerium salt, extremely viscous gel-like systems are even formed. Such transformations are significantly accelerated in solutions that have undergone electrochemical investigations (cyclic scanning of the electrode potential on a platinum electrode): after current passage and additional CeO_2 accumulation via electrochemical reactions, turbidity is observed within just 1–2 days after the experiments (depending on the Ce(III) salt concentration, the total charge passed, the number of potential scans, etc.). At the same time, it should be noted that in long-term experiments (several hours) of galvanostatic electrolysis using $CeCl_3 \cdot 7H_2O$ solutions in reline, neither during cathodic current passage nor under anodic polarization was the formation of any firmly adherent coating on the electrode surface observed.

Thus, during the electrolysis of cerium(III) salt solutions in DES, the formation of a colloidal dispersion of cerium dioxide is possible via the corresponding anodic process, in addition to the chemical pathway of this process (reactions (7)–(10)). However, CeO_2 particles are electrochemically active and, during the cathodic potential scan, can undergo electrochemical reduction, producing the corresponding current wave in the CVs.

Journal of Chemistry and Technologies, 2025, *33*(4), 1026-1044

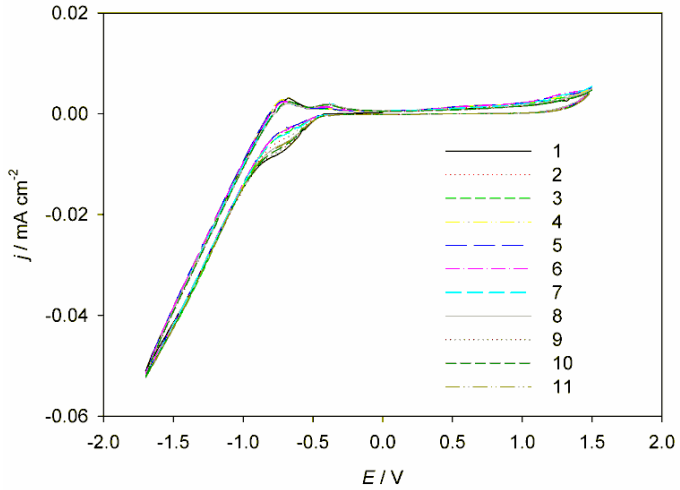

Fig. 4. Cyclic voltammograms of a platinum electrode in reline + 0.2 M Ce(III) during consecutive multiple potential scans (100 mV/s, 70°C). The numbers indicate the sequence of scan cycles

Figure 5 shows the cyclic voltammograms for an electrolyte containing dissolved nickel(II) salt in reline. The limiting current wave corresponding to the nickel deposition reaction (reaction (4)) appears in the potential range of –0.5 to –1.0 V, overlapping, upon further potential sweep, with the cathodic reduction wave of the eutectic solvent components. On the reverse (anodic) scan, the current wave attributed to the anodic dissolution of nickel deposited on platinum is observed at potentials of approximately 0 to 0.5 V. This wave splits into two weak, overlapping peaks, which are clearly distinguishable only during the first potential scan cycle. Overall, such a shape of the cathodic-anodic waves for nickel deposition-dissolution in reline is typical and has been repeatedly reported in the literature [45–47]. Those publications discussed in detail the possible reasons for the splitting of the nickel dissolution anodic wave in DESs into two peaks; therefore, these issues are not considered in detail in the present study.

An interesting feature of the CVs obtained in the $NiCl_2 \cdot 6H_2O$ solution in reline is the pronounced hysteresis of successive potential scans. The highest cathodic deposition currents and, accordingly, the largest anodic nickel dissolution currents are observed during the first scan, while in the second and subsequent consecutive scans the currents decrease, reaching a certain quasi-steady-state value by approximately the 6th-7th potential cycling scan. Beyond this point, the shape of the voltammetric curves remains practically unchanged. This specific behavior, which indicates a kind of gradual catalytic "poisoning" of the surface, was described in our previous work [29], where it was suggested that the effect may be caused by the gradual accumulation on the surface of adsorbed products that partially passivate it, for example, $Ni(OH)_{2(ads)}$ [36].

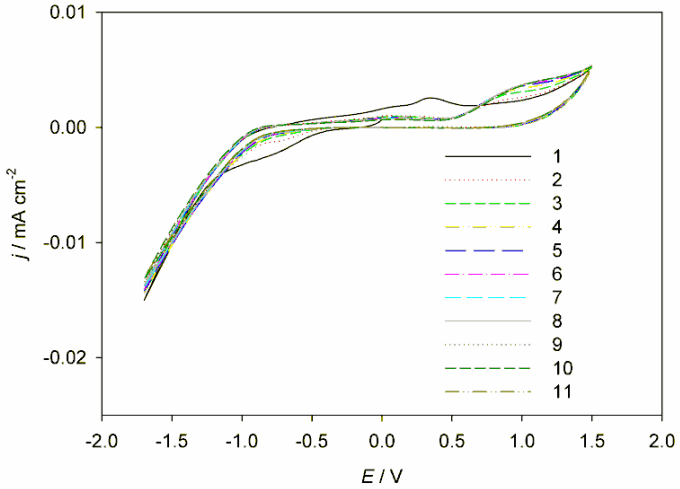

Fig. 5. Cyclic voltammograms of a platinum electrode in reline + 0.3 M Ni(II) during consecutive multiple potential scans (100 mV/s, 70°C). The numbers indicate the sequence of scan cycles

Journal of Chemistry and Technologies, 2025, *33*(4), 1026-1044

In the simultaneous presence of dissolved $NiCl_2 \cdot 6H_2O$ and $CeCl_3 \cdot 7H_2O$ salts in reline, the CVs (Fig. 6) naturally exhibit all the characteristic cathodic and anodic current waves observed in the CVs recorded for solutions containing only cerium salt or only nickel salt individually. At the same time, as follows from the analysis of the curves in Figs. 4–6, the cathodic waves corresponding to the electroreduction of Ce(IV) compounds to Ce(III) and Ni(II) to Ni(0) are not separated on the CVs but instead form a single combined current wave, since these processes occur within nearly the same potential range (approximately –0.6 to –1.0 V). A similar situation is observed for the reverse electrode processes (oxidation of Ni(0) and oxidation of Ce(III) compounds): they yield a single broad anodic current wave on the CVs (approximately from –0.5 to +0.8 V).

As in the case of the reline solution containing only dissolved nickel salt, in the simultaneous presence of Ni(II) and Ce(III) salts, the first potential scan exhibits markedly higher currents across almost the entire CV compared with all subsequent scans, whose curves nearly coincide, indicating the establishment of a quasi-stationary state for the electrode reactions.

It is also noteworthy that the anodic dissolution currents of nickel are significantly higher when cerium is simultaneously present in the electrolyte. In other words, the voltammetric curves shown in Fig. 6 are clearly not a simple additive combination of those in Figs. 4 and 5, as might be expected from the principle of independent electrochemical reactions. Instead, the observed currents are considerably higher, indicating a specific type of anomalous nickel deposition that is synergistically accelerated by the simultaneous occurrence of electrochemical reactions involving cerium compounds at the electrode. It is likely that intermediate cerium hydroxide compounds, which inevitably form *in situ* in the near-electrode layer during the deposition of Ni-based composites, act as additional catalytic sites that facilitate charge transfer during the discharge of Ni(II) ions. This explanation is consistent with current understanding of the catalytic role of hydroxide ions and hydroxide compounds in the electrodeposition of iron-group metals (including nickel) [48]. It is also possible that cerium, which can exist in multiple oxidation states, exerts an electrocatalytic effect on nickel deposition as a charge carrier, for example, through the operation of the Ce(IV)/Ce(III) redox couple.

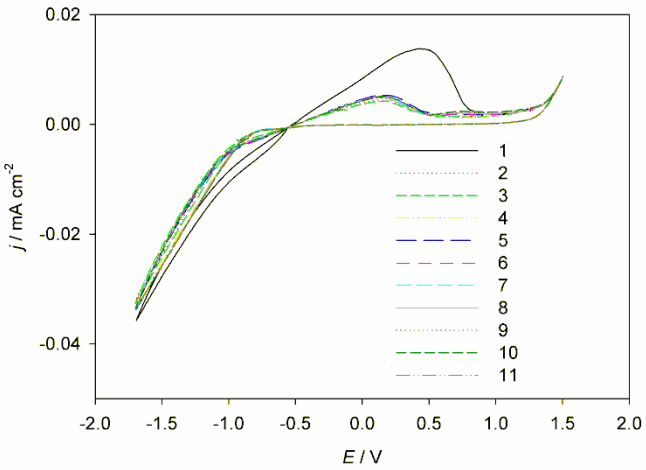

Fig. 6. Cyclic voltammograms of a platinum electrode in reline + 0.3 M Ni(II) + 0.2 M Ce(III) during consecutive multiple potential scans (100 mV/s, 70°C). The numbers indicate the sequence of scan cycles

Evaluation of the electrocatalytic activity of the deposited coatings toward reactions (1)–(3) was carried out by recording cyclic voltammograms in aqueous solutions of 1 M NaOH and 1 M NaOH + 0.33 M $CO(NH_2)_2$ (Figs. 7–10). It should be noted that the curves presented in these figures were recorded on the tenth consecutive potential scan cycle, when their shape practically ceases to change after each subsequent cycle [29].

The voltammetric curves recorded in the alkaline 1 M NaOH solution without urea addition show several characteristic regions: cathodic hydrogen evolution at potentials more negative than approximately –1.1 V, and anodic oxygen evolution at potentials more positive than approximately 0.6 V (Fig. 7). Additionally, anodic-cathodic current waves appear at around 0.2 to 0.5 V, which, according to literature data [49], correspond to electrochemical transformations of

Journal of Chemistry and Technologies, 2025, *33*(4), 1026-1044

Ni(II)⇔Ni(III) in the redox system $Ni(OH)_2$/NiOOH.

As can be seen, the concentration of nickel(II) salt in the electrolyte used for coating deposition significantly affects the current densities across all regions of the cyclic voltammograms under consideration. In particular, the overpotentials for both hydrogen and oxygen evolution are substantially reduced when the $NiCl_2 \cdot 6H_2O$ concentration decreases from 0.3 to 0.2 mol/dm³. It is noteworthy that, simultaneously, the peak currents of the anodic and cathodic waves corresponding to the redox transitions between Ni(II) and Ni(III) hydroxide compounds increase markedly. According to the data in Table 1, coatings deposited from the solution containing 0.2 mol/dm³ Ni(II) have a higher oxygen content, and presumably a greater amount of nickel hydroxide compounds, than those deposited from the solution with 0.3 mol/dm³ Ni(II). In other words, there is a certain correlation between the peak height and the area under the curve corresponding to the anodic-cathodic transitions in the $Ni(OH)_2$/NiOOH system and the electrocatalytic activity toward both hydrogen and oxygen evolution reactions, as was previously noted in reference [29].

Thus, increasing the concentration of electrochemically active nickel oxide–hydroxide compounds with variable oxidation states in the coating, achieved by decreasing the concentration of nickel(II) salt in the reline-based deposition electrolyte, leads to a pronounced enhancement of the electrocatalytic activity toward all electrode processes occurring on the coating in an aqueous 1 M NaOH solution. This is likely associated with an increase in the concentration and activity of electrocatalytic redox sites on a more defective surface, which consists of a mixture of hydroxide phases and metallic nanocrystalline nickel. Such an effect is an important factor for the targeted enhancement of the electrocatalytic activity of materials electrochemically synthesized from DES-based solutions.

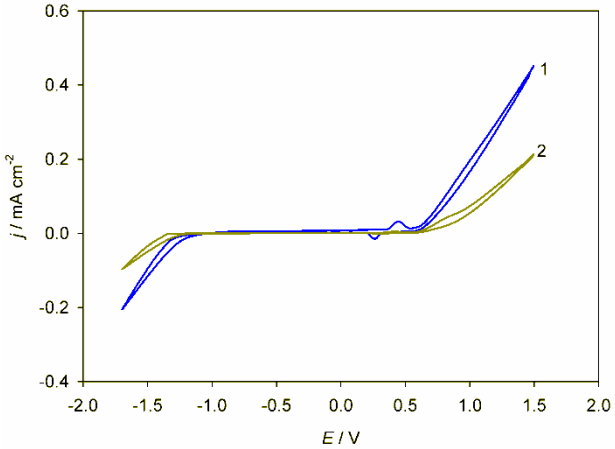

Fig. 7. Cyclic voltammograms of an electrode with a deposited coating in an aqueous 1 M NaOH solution (50 mV/s, 25 °C). The coatings were deposited from a $NiCl_2 \cdot 6H_2O$ salt solution in reline at a current density of 3 mA/cm² and a temperature of 70°C. Ni(II) concentration, mol/dm³: 1 – 0.2; 2 – 0.3

The introduction of cerium(III) salt into the reline-based electrolyte containing dissolved nickel(II) salt significantly affects the electrocatalytic properties of the resulting coatings (Fig. 8) and somewhat complicates the shape of the corresponding CVs. Notably, an additional anodic wave appears in the recorded CVs at potentials of approximately –1.0 to –0.5 V. We assume that this anodic current is associated with the oxidation of cerium compounds that were partially electrochemically reduced during the preceding cathodic scan. As can be seen, the height of this anodic peak and the corresponding area under the voltammetric curve slightly increase with increasing nickel salt concentration in the deposition solution, which correlates with the corresponding increase in cerium content in the coating (Table 1).

It is interesting to note that analysis of the CVs presented in Fig. 8 reveals that the anodic waves corresponding to the redox transitions in the $Ni(OH)_2$/NiOOH system for nickel-cerium-containing coatings deposited at different nickel(II) salt concentrations (0.2 and 0.3 mol/dm³) are nearly identical, indicating an approximately equal surface concentration of these electroactive compounds. Accordingly, the CV regions corresponding to hydrogen evolution also coincide almost completely, while those associated with oxygen evolution are quite close to each other, suggesting similar electrocatalytic responses.

Journal of Chemistry and Technologies, 2025, *33*(4), 1026-1044

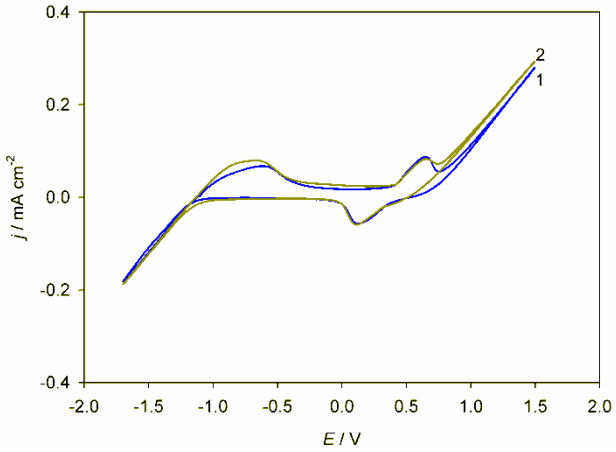

Fig. 8. Cyclic voltammograms of an electrode with the deposited coating in an aqueous 1 M NaOH solution (50 mV/s, 25°C). The coatings were deposited from a solution of $NiCl_2 \cdot 6H_2O$ (0.2 and 0.3 mol/dm³) and $CeCl_3 \cdot 7H_2O$ (0.5 mol/dm³) in reline at a current density of 3 mA/cm² and a temperature of 70°C. Ni(II) concentration, mol/dm³: 1 – 0.2; 2 – 0.3

It is important to analyze how the incorporation of cerium into the coating affects electrocatalytic behavior at the same nickel salt concentration in the deposition electrolyte. To this end, the corresponding cyclic curves from Figs. 7 and 8 were paired and compared in Fig. 9a,b.

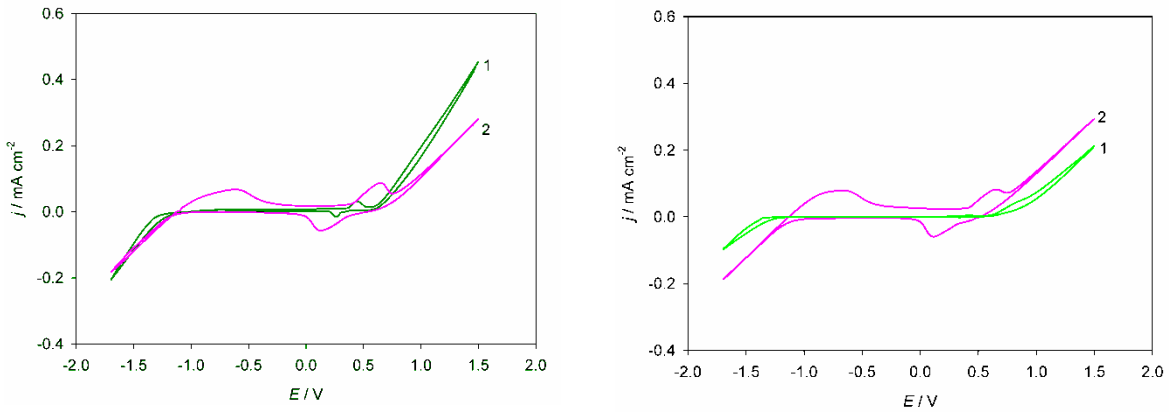

Fig. 9. Cyclic voltammograms of an electrode with the deposited coating in an aqueous 1 M NaOH solution (50 mV/s, 25 °C). Coatings were deposited at a current density of 3 mA/cm² and a temperature of 70°C. Ni(II) concentration, mol/dm³: (a) 0.2; (b) 0.3. Ce(III) concentration, mol/dm³: 1 – 0; 2 – 0.5

It can be seen that the incorporation of cerium compounds into the nickel matrix, for both Ni(II) salt concentrations used, results in a significant increase in the height and area of the peaks associated with the Ni(II)⇔Ni(III) redox transformation. Thus, the formation of cerium oxide in the near-electrode layer promotes an increase in the surface concentration of nickel hydroxide, which is consistent with the X-ray diffraction data (Fig. 2). However, the effect of the incorporated cerium oxide on the electrocatalytic behavior varies depending on both the type of reaction considered and the Ni(II) salt concentration in the deposition electrolyte. In particular, at a Ni(II) concentration of 0.2 mol/dm³ (Fig. 9a), the inclusion of cerium oxide in the coating has little influence on the kinetics of the hydrogen evolution reaction, while noticeably increasing the overpotential of the oxygen evolution reaction (i.e., reducing electrocatalytic activity). In contrast, at a Ni(II) concentration of 0.3 mol/dm³ (Fig. 9b), coatings containing incorporated cerium oxide exhibit a pronounced decrease in the overpotential for both the hydrogen and oxygen evolution reactions compared to the cerium-free coating.

Such rather complex and ambiguous behavior can be explained, on the one hand, by differences in the mechanisms of the multistep hydrogen and oxygen evolution processes, which involve distinct intermediate compounds and, accordingly, different types of active sites on the surface. These processes also occur under markedly different adsorption conditions on the

Journal of Chemistry and Technologies, 2025, *33*(4), 1026-1044

electrode and feature specific structures of the electrical double layer, due to the significantly different potential ranges in which they take place. On the other hand, the observed phenomena indicate that cerium-containing compounds themselves can act as electrocatalytically active sites on the surface, exerting a synergistic yet multifaceted influence on the electrocatalytic activity of nickel-based active sites. Nevertheless, the revealed effects open the possibility for a sufficiently flexible tuning of the electrocatalytic performance and catalytic selectivity of the coatings by varying the concentrations of nickel and cerium salts during coating deposition.

On the curves reflecting the electrochemical behavior of the deposited coatings in an aqueous solution of 1 M NaOH with the addition of 0.33 M $CO(NH_2)_2$ (Figs. 10 and 11), anodic current waves appear, which are caused by the electrochemical oxidation of urea at potentials of approximately 0.4 ... 0.8 V [29]. It is worth noting that the foot of this current wave exactly coincides with the corresponding region of anodic transformation of surface nickel hydroxide compounds of various oxidation states $Ni(OH)_2 \Leftrightarrow NiOOH$. This coincidence is not accidental, as current understanding indicates that NiOOH acts as the electrocatalytic site on the surface during the electrooxidation of urea [8]. Specifically, according to the so-called direct mechanism, adsorbed $CO(NH_2)_2$ molecules react with hydroxide ions to produce the final reaction products, gaseous N_2 and CO_2:

$$Ni(OH)_2 + OH^- \rightarrow NiOOH + H_2O + e^- \quad (13)$$

$$CO(NH_2)_2 + 6OH^- \xrightarrow{NiOOH} N_2 + CO_2 + 5H_2O + 6e^- \quad (14)$$

The indirect mechanism [50] assumes that $Ni(OH)_2$ is electrochemically oxidized to NiOOH (as in the direct mechanism), and then directly interacts with the adsorbed $CO(NH_2)_2$ molecules:

$$6NiOOH + CO(NH_2)_2 + H_2O \rightarrow 6Ni(OH)_2 + N_2 + CO_2. \quad (15)$$

It is clear that both mechanisms can only occur within the potential range where the electrocatalyst regeneration is possible through the anodic oxidation of $Ni(OH)_2$ to form NiOOH; thus, the redox potential of this reaction defines the potential region on the voltammogram where urea oxidation takes place. It should be noted that based on the data obtained in this study, it is not possible to differentiate between the direct and indirect reaction mechanisms in this case. It is likely that both mechanisms may be involved simultaneously.

It can probably be stated that one of the important factors determining the rate of electrochemical urea oxidation is the surface concentration of the electroactive forms of the Ni(II)⇔Ni(III) catalyst. Indeed, there is a certain parallelism between the data in Figures 7 and 10, the comparison of which shows that decreasing the concentration of nickel salt in the electrolyte used for electrodepositing the electrocatalytic coating from 0.3 to 0.2 mol/dm³ results in an increase in the currents corresponding both to the redox transitions in the Ni(II)⇔Ni(III) couple and to those associated with the catalytic oxidation of urea molecules.

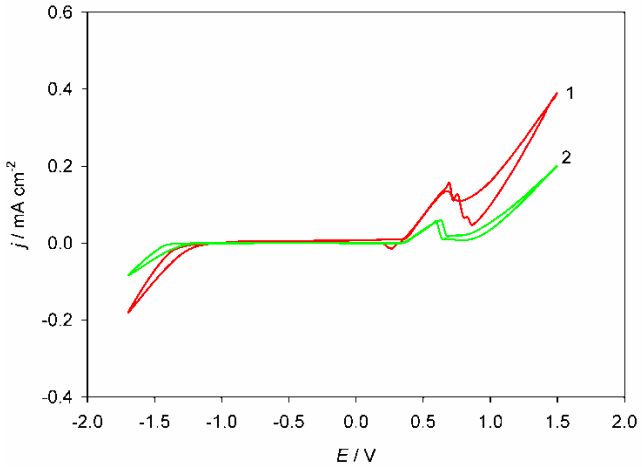

Fig. 10. Cyclic voltammograms of the electrode with the deposited coating in an aqueous solution of 1 M NaOH + 0.33 M $CO(NH_2)_2$ (50 mV/s, 25°C). The coatings were deposited from a solution of $NiCl_2 \cdot 6H_2O$ (0.2 and 0.3 mol/dm³) in reline at a current density of 3 mA/cm² and a temperature of 70°C. Ni(II) concentration, mol/dm³: 1 – 0.2; 2 – 0.3

However, upon transitioning to the nickel-cerium-containing electrocatalyst, the observed phenomena become more complex, as mentioned above (Fig. 11). The CV curves characterizing the electrochemical responses of the Ni-based composite coatings in a 1 M NaOH + 0.33 M $CO(NH_2)_2$ solution (the figure shows curves for the highest cerium salt concentration used in the deposition electrolyte, 0.5 mol/dm^3; curves for other concentrations exhibit similar behavior and are not shown here) display all the characteristic features observed in the curves from Figs. 7 and 10. A noticeable decrease in the hydrogen evolution overpotential is observed upon incorporation of cerium compounds into the deposited coating. Furthermore, there is a significant increase in the current densities corresponding to the urea oxidation reaction on the CVs (in the potential range of 0.4 ... 1.0 V), indicating enhanced electrocatalytic activity.

To quantitatively compare the effect of the concentrations of the deposition electrolyte components (Ni(II) and Ce(III) salts), and thus the composition of the formed coating, on the electrocatalytic characteristics regarding the urea oxidation reaction (2), we used two parameters: the anodic current density in the 1 M NaOH + 0.33 M $CO(NH_2)_2$ solution at 0.6 V, where this electrode reaction proceeds almost quantitatively [29; 51], and the maximum current density observed at the anodic peak (recorded under specific voltammetric conditions, without referencing the potential value corresponding to this maximum current). Both parameters were extracted from the forward anodic scans (i.e., when moving from negative to positive potentials) of the CV curves, and their values for various compositions of the electrocatalytic coatings deposition electrolytes are summarized in Table 2.

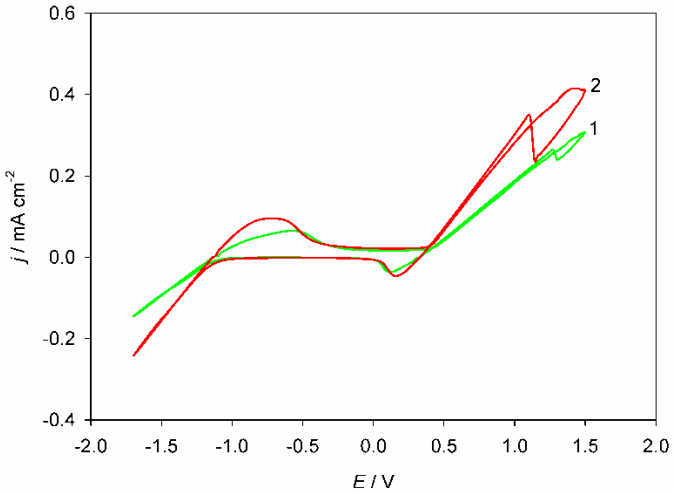

Fig. 11. Cyclic voltammograms of the electrode with deposited coating in an aqueous solution of 1 M NaOH + 0.33 M $CO(NH_2)_2$ (50 mV/s, 25°C). The coatings were deposited from a solution containing $NiCl_2 \cdot 6H_2O$ (0.2 and 0.3 mol/dm^3) and $CeCl_3 \cdot 7H_2O$ (0.5 mol/dm^3) in reline at a current density of 3 mA/cm^2 and a temperature of 70°C. Concentration of Ni(II), mol/dm^3: 1 – 0.2; 2 – 0.3

Table 2

Effect of Ni(II) and Ce(III) ion concentrations in the reline-based deposition electrolyte on the anodic current density of the urea oxidation reaction

Content of the main components in the deposition electrolyte		Parameters of the urea electrooxidation reaction	
concentration of Ni(II) ions, mol/dm^3	concentration of Ce(III)) ions, mol/dm^3	anodic current density at 0.6 V, mA/cm^2	maximum achieved anodic current density for urea oxidation, mA/cm^2
0.2	–	0.116	0.155
	0.2	0.093	– *
	0.3	0.117	0.466
	0.4	0.097	– *
	0.5	0.075	0.263
0.3	–	0.056	0.058
	0.2	0.132	0.324
	0.3	0.112	0.316
	0.4	0.087	0.272
	0.5	0.117	0.350

Note: * – The peak current value on the voltammetric curve cannot be determined because the oxidation waves of urea and oxygen evolution overlap and are not distinguishable.

Journal of Chemistry and Technologies, 2025, *33*(4), 1026-1044

As can be seen, overall the electrocatalytic activity of the coating tends to increase with the incorporation of cerium compounds, especially noticeable in the case when the coating was deposited from an electrolyte containing 0.3 mol/dm^3 nickel salt: the anodic current densities at a potential of 0.6 V significantly increase upon the incorporation of cerium oxide into the coating. However, no clear trends are observed between the electrocatalytic activity parameters listed in Table 2 and the cerium compound content in the coatings (Table 1).

Regarding the nature of the stimulating effect of incorporating CeO_2 particles into the nickel matrix on the electrocatalytic activity in the urea oxidation reaction, it is likely that the mechanism of the process remains unchanged, and the transformations occur at the nickel-containing electrocatalytic sites. This is supported, in particular, by the invariance of the potential ranges at which this reaction proceeds, which, as noted above, are determined by the thermodynamics and kinetics of the Ni(II)⇔Ni(III) redox transformations.

The positive effect of dopant elements on the electrooxidation of urea reactions on nickel-based electrocatalysts is generally attributed in the literature to factors such as the formation of a more heterogeneous nanostructured surface with a higher concentration of active sites, as well as synergistic structural and electronic effects at the nanoscale, stabilization of intermediates, and enhanced adsorption of urea molecules [52]. It has also been established [53] that anchored sites from "foreign" transition metal atoms effectively support the generation of dynamic active NiOOH sites, thereby further promoting the urea decomposition process. Likely, all these factors are also responsible for the effects observed upon incorporation of cerium dioxide into the nickel matrix electrodeposited from DES. However, in addition to the factors mentioned, structural and morphological aspects probably influence the electrocatalytic activity as well (in particular, the evolution of the surface microprofile upon incorporation of cerium compounds into the electrocatalytic coating, as evidenced by the data in Fig. 1). The combined influence of a whole range of diverse factors likely determines the rather complex and clearly non-monotonic character of the effect of electrolyte composition, and thus the chemical composition of the coating, on its electrocatalytic behavior in hydrogen and oxygen evolution reactions as well as urea electrooxidation. Nevertheless, it is important that under certain conditions it is possible to significantly improve the electrocatalytic performance, thereby enabling controlled tuning of the activity and selectivity of electrochemically deposited multifunctional electrocatalysts.

Conclusions

1. It has been demonstrated that composite coatings containing cerium dioxide incorporated into a nanocrystalline nickel matrix can be electrochemically deposited from an electrolyte based on a deep eutectic solvent composed of choline chloride and urea (reline), which contains dissolved salts $NiCl_2{\cdot}6H_2O$ and $CeCl_3{\cdot}7H_2O$. The incorporation of CeO_2 into the nickel deposit leads to the evolution of surface morphological patterns and an increase in surface defects, which is expected to contribute to enhanced electrocatalytic activity.

2. Using cyclic voltammetry with consecutive multiple potential scans, it was found that on a platinum electrode in the reline-based solution, the potential ranges of the electroreduction reactions of nickel and cerium compounds overlap. A reaction scheme for the processes occurring during the formation of the composite coating is proposed, involving a series of both electrochemical reactions and chemical processes within the electrolyte near-electrode layer.

3. Electrochemically deposited Ni-based composite coatings were tested as potential electrocatalysts for hydrogen and oxygen evolution reactions in aqueous 1 M NaOH, as well as for the anodic urea oxidation reaction in 1 M NaOH + 0.33 M $CO(NH_2)_2$ solution. The latter is considered in the literature as a promising alternative to the oxygen evolution reaction during water electrolysis in alkaline media, aiming to reduce energy consumption. It was shown that the incorporation of cerium into the nickel electrodeposited matrix under certain conditions (specific concentrations of Ni(II) and Ce(III) salts in the deposition electrolyte) promotes selective enhancement of the electrocatalytic activity of the coatings for all three studied reactions.

4. Ni-based composite coatings containing cerium compounds electrodeposited from deep eutectic solvent-assisted electrolytes can be considered as promising multifunctional electrocatalysts for green hydrogen generation in hydrogen energy applications. Variation of Ni(II) and Ce(III) salt concentrations in the DES-based deposition bath enables flexible and controlled tuning of the electrocatalytic behavior.

Acknowledgments

This work was supported by the Ministry of Education and Science of Ukraine under project no. 0124U000563.

References

[1] Dawood, F., Anda, M., Shafiullah, G. M. (2020). Hydrogen production for energy: An overview. *Int. J. Hydrogen Energy*, *45*, 3847–3869. https://doi.org/10.1016/j.ijhydene.2019.12.059

[2] Shih, A. J., Monteiro, M. C. O., Dattila, F., Pavesi, D., Philips, M., da Silva, A. H. M., Vos. R. E, Ojha, K., Park, S., van der Heijden, O., Marcandalli, G., Goyal, A., Villalba, M., Chen, X., Gunasooriya, G. T. K. K., McCrum, I., Mom, R., López, N., Koper, M. T. M. (2022). Water electrolysis. *Nat. Rev. Methods Primers*, *2*, 84. https://doi.org/10.1038/s43586-022-00164-0

[3] Squadrito, G., Maggio, G., Nicita, A. (2023). The green hydrogen revolution. *Renewable Energy*, *216*, 119041. https://doi.org/10.1016/j.renene.2023.119041

[4] Qadeer, M. A., Zhang, X., Farid, M. A., Tanveer, M., Yan, Y., Du, S., Huang, Z. F., Tahir, M., Zou, J.J. (2024). A review on fundamentals for designing hydrogen evolution electrocatalyst. *J. Power Sources*, 613, 234856. https://doi.org/10.1016/j.jpowsour.2024.234856

[5] Zhou, W., Chen, S., Meng, X., Li, J., Gao, J. (2023). Energy-saving cathodic H_2 production enabled by non-oxygen evolution anodic reactions: A critical review on fundamental principles and applications. *Int. J. Hydrogen Energy*, *48*, 15748–15770. https://doi.org/10.1016/j.ijhydene.2023.01.063

[6] Paygozar, S., Aghdam, A. S. R., Hassanizadeh, E., Andaveh, R., Darband, G. B. (2023). Recent progress in non-noble metal-based electrocatalysts for urea-assisted electrochemical hydrogen production. *Int. J. Hydrogen Energy*, *48*, 7219–7259. https://doi.org/10.1016/j.ijhydene.2022.11.087

[7] Anuratha, K.S., Rinawati, M., Wu, T.H., Yeh, M.H., Lin, J.Y. (2022). Recent development of nickel-based electrocatalysts for urea electrolysis in alkaline solution. *Nanomaterials*, *12*, 2970. https://doi.org/10.3390/nano12172970

[8] Boggs, B. K., King, R. L., Botte, G. G. (2009). Urea electrolysis: direct hydrogen production from urine. *Chem Commun*., 4859–4861. https://doi.org/10.1039/b905974a

[9] Protsenko, V. S. (2023). Thermodynamic aspects of urea oxidation reaction in the context of hydrogen production by electrolysis. *Int. J. Hydrogen Energy*, *48*, 24207–24211. https://doi.org/10.1016/j.ijhydene.2023.03.295

[10] Protsenko, V. S., Bobrova, L. S., Butyrina, T. E., Sukhatskyi, O. D. (2024). Thermodynamics of electrochemical urea oxidation reaction coupled with cathodic hydrogen evolution reaction in an alkaline solution: Effect of carbonate formation. *Int. J. Hydrogen Energy*, *59*, 354–358. https://doi.org/10.1016/j.ijhydene.2024.02.006

[11] Li, J., Zhang, J., Yang, J. H. (2022). Research progress and applications of nickel-based catalysts for electrooxidation of urea. *Int. J Hydrogen Energy*, *47*, 7693–7712. https://doi.org/10.1016/j.ijhydene.2021.12.099

[12] Lu, S., Zheng, X., Fang, L., Yin, F., Liu, H. (2023). Rational engineering design of nickel hydroxides for urea oxidation reaction: A mini-review. *Electrochem. Commun*., *157,* 107599. https://doi.org/10.1016/j.elecom.2023.107599

[13] Ge, J., Liu, Z., Guan, M., Kuang, J., Xiao, Y., Yang, Y., Tsang, C. H., Lu, X., Yang, C. (2022). Investigation of the electrocatalytic mechanisms of urea oxidation reaction on the surface of transition metal oxides. *J. Colloid Interface Sci*., *620*, 442–453. https://doi.org/10.1016/j.jcis.2022.03.152

[14] Sun, X., Ding, R. (2020). Recent progress with electrocatalysts for urea electrolysis in alkaline media for energy-saving hydrogen production. *Catal. Sci. Technol*., *10*, 1567–1581. https://doi.org/10.1039/C9CY02618E

[15] Yang, K., Hao, L., Hou, Y., Zhang, J., Yang, J. H. (2024). Summary and application of Ni-based catalysts for electrocatalytic urea oxidation. *Int. J. Hydrogen Energy*, *51*, 966–981. https://doi.org/10.1016/j.ijhydene.2023.10.279

[16] Li, R., Li, Y., Yang, P., Wang, D., Xu, H., Wang, B., Meng, F., Zhang, J., An, M. (2021). Electrodeposition: synthesis of advanced transition metal-based catalyst for hydrogen production via electrolysis of water. *J. Energy Chem*., *57*, 547–566. https://doi.org/10.1016/j.jechem.2020.08.040

[17] Wang, H., Jiao, X., Zeng, W., Zhang, Y., Jiao, Y. (2021). Electrodeposition NiMoSe ternary nanoshperes on nickel foam as bifunctional electrocatalyst for urea electrolysis and hydrogen evolution reaction. *Int. J. Hydrogen Energy*, 46, 37792–37801. https://doi.org/10.1016/j.ijhydene.2021.09.050

[18] Abd El-Lateef, H. M., Almulhim, N. F., Mohamed, I. M. A. (2020). Physicochemical and electrochemical investigations of an electrodeposited $CeNi_2$@NiO nanomaterial as a novel anode electrocatalyst material for urea oxidation in alkaline media. *J. Mol. Liq*., *297*, 111737. https://doi.org/10.1016/j.molliq.2019.111737

[19] Kityk, A., Pavlik, V., Hnatko, M. (2023). Exploring deep eutectic solvents for the electrochemical and chemical synthesis of photo- and electrocatalysts for hydrogen evolution. *Int. J. Hydrogen Energy*, *48*, 39823–39853. https://doi.org/10.1016/j.ijhydene.2023.07.158

[20] Al-Farsi, R., Hayyan, M. (2024). Deep eutectic solvents: Green multi-task agents for sustainable super green hydrogen technologies. *J. Energy Chem*., *92*, 357–382. https://doi.org/10.1016/j.jechem.2023.12.021

[21] Kityk, A., Pavlik, V., Hnatko, M. (2024). Breaking barriers in electrodeposition: Novel eco-friendly approach based on utilization of deep eutectic solvents. *Adv. Colloid Interface Sci*., *334*, 103310. https://doi.org/10.1016/j.cis.2024.103310

[22] Smith, E. L., Abbott, A. P., Ryder, K. S. (2014). Deep eutectic solvents (DESs) and their applications. *Chem. Rev*., *114*, 11060–11082. https://doi.org/10.1021/cr300162p

[23] Hansen, B. B., Spittle, S., Chen, B., Poe, D., Zhang, Y., Klein, J. M., Horton, A., Adhikari, L., Zelovich, T., Doherty, B. W., Gurkan, B., Maginn, E. J., Ragauskas, A., Dadmun, M., Zawodzinski, T. A., Baker, G. A., Tuckerman, M. E., Savinell, R. F., Sangoro, J. R. (2021). Deep eutectic solvents: a review of fundamentals and

applications. *Chem. Rev*., *121*, 1232–1285. https://doi.org/10.1021/acs.chemrev.0c00385

[24] Abbott, A. P. (2022). Deep eutectic solvents and their application in electrochemistry. *Curr. Opin. Green Sustainable Chem*., *36*, 100649. https://doi.org/10.1016/j.cogsc.2022.100649

[25] Zhang, C., Fu, Y., Gao, W., Bai, T., Cao, T., Jin, J., Xin, B. (2022). Deep eutectic solvent-mediated electrocatalysts for water splitting. *Molecules*, *27*, 8098. https://doi.org/10.3390/molecules27228098

[26] Zhang, C., Bai, T., Sun, Y., Xin, B., Zhang, S. (2022). Ionic liquid/deep eutectic solvent-mediated Ni-based catalysts and their application in water splitting electrocatalysis. *Catalysts*, *12*, 928. https://doi.org/10.3390/catal12080928

[27] Wang, H., Kang, X., Han, B. (2024). Electrocatalysis in deep eutectic solvents: from fundamental properties to applications. *Chem. Sci*., *15*, 9949–9976. https://doi.org/10.1039/d4sc02318h

[28] Kityk, A. A., Shaiderov, D. A., Vasil'eva, E. A., Protsenko, V. S., Danilov, F. I. (2017). Choline chloride based ionic liquids containing nickel chloride: Physicochemical properties and kinetics of Ni(II) electroreduction. *Electrochim. Acta*, *245*, 133–145. http://dx.doi.org/10.1016/j.electacta.2017.05.144

[29] Protsenko, V. S., Shaiderov, D. A., Sukhatskyi, O. D., Butyrina, T. E., Korniy, S. A. (2025). Nickel-containing electrocatalysts for green hydrogen production: electrodeposition from deep eutectic solvent-based solutions and electrocatalytic activity for hydrogen evolution, oxygen evolution and urea oxidation reactions. *J. Appl. Electrochem*., *55,* 2129–2148. https://doi.org/10.1007/s10800-025-02288-z

[30] Protsenko, V. S., Butyrina, T. E., Danilov, F. I. (2022). Kinetics and mechanism of electrochemical oxygen evolution in an alkaline solution on nickel coatings. *J. Chem. Technol*., *30*(1), 26–33. https://doi.org/10.15421/jchemtech.v30i1.245490

[31] Protsenko, V. S., Pavlenko, L. M., Bobrova, L. S., Korniy, S. A., Danilov, F. I. (2024). Electrodeposition of coatings from urea–choline chloride-based plating baths containing Ni(II) and Ce(III) chloride salts and electrocatalytic activity of electrodeposits towards the hydrogen evolution reaction. *J. Solid State Electrochem*., *28*, 1641–1655. https://doi.org/10.1007/s10008-023-05499-6

[32] Protsenko, V. S., Shaiderov, D. A., Sukhatskyi, O. D., Butyrina, T. E., Korniy, S. A., Danilov, F. I. (2025). DES-assisted electrodeposition and characterization of an electrocatalyst for enhanced urea oxidation in green hydrogen production. *Voprosy Khimii i Khimicheskoi Tekhnologii*, (1), 65–70. https://doi.org/10.32434/0321-4095-2025-158-1-65-70

[33] Protsenko, V. S., Bobrova, L. S., Butyrina, T. E., Baskevich, A. S., Korniy, S. A., Danilov, F. I. (2023). Electrodeposited Ni–Mo coatings as electrocatalytic materials for green hydrogen production. *Heliyon*, *9*, e15230. https://doi.org/10.1016/j.heliyon.2023.e15230

[34] Wang, S., Zou, X., Lu, Y., Rao, S., Xie, X., Pang, Z., Lu, X., Xu, Q., Zhou, Z. (2018). Electrodeposition of nano-nickel in deep eutectic solvents for hydrogen evolution reaction in alkaline solution. *Int J Hydrogen Energy*, 43, 15673–15686. https://doi.org/10.1016/j.ijhydene.2018.06.188

[35] Lukaczynska, M., Cherigui, E. A. M., Ceglia, A., Van Den Bergh, K., De Strycker, J., Terryn, H., Ustarroz, J. (2019). Influence of water content and applied potential on the electrodeposition of Ni coatings from deep eutectic solvents. *Electrochim. Acta*, *319*, 690–704. https://doi.org/10.1016/j.electacta.2019.06.161

[36] Phi, T. L., Nguyen, S. T., Hieu, N. V., Palomar-Pardavé, M., Morales-Gil, P., Le Manh, T. (2022). Insights into electronucleation and electrodeposition of nickel from a non-aqueous solvent based on $NiCl_2{\cdot}6H_2O$ dissolved in ethylene glycol. *Inorg. Chem.*, *61*, 5099–5111. https://doi.org/10.1021/acs.inorgchem.2c00127

[37] Hasannejad, H., Shahrabi, T., Jafarian, M., Rouhaghdam, A. S. (2011). EIS study of nano crystalline Ni-cerium oxide coating electrodeposition mechanism. *J. Alloys Compd*., *509*, 1924–1930. https://doi.org/10.1016/j.jallcom.2010.10.089

[38] Hassannejad, H., Mele, C., Shahrabi, T., Bozzini, B. (2012). Electrodeposition of Ni/ceria composites: an in situ visible reflectance investigation. *J. Solid State Electrochem*., *16*, 3429–3441. https://doi.org/10.1007/s10008-012-1830-4

[39] Hasannejad, H., Shahrabi, T. (2012). Economical deposition of Ni high cerium oxide nanocomposite coatings. *Surf. Eng.*, *28*, 418–423. https://doi.org/10.1179/1743294411Y.0000000086

[40] Hamlaoui, Y., Pedraza, F., Remazeilles, C., Cohendoz, S., Rebere, C., Tifouti, L., Creus, J. (2009). Cathodic electrodeposition of cerium-based oxides on carbon steel from concentrated cerium nitrate solutions. Part I. Electrochemical and analytical characterisation. *Mater. Chem. Phys.*, *113*, 650–657. https://doi.org/10.1016/j.matchemphys.2008.08.027

[41] Protsenko, V. S., Vasil'eva, E. A., Tsurkan, A. V., Kityk, A. A., Korniy, S. A., Danilov, F. I. (2017). Fe/TiO_2 composite coatings modified by ceria layer: Electrochemical synthesis using environmentally friendly methanesulfonate electrolytes and application as photocatalysts for organic dyes degradation. *J. Environ. Chem. Eng*., 5, 136–146. https://doi.org/10.1016/j.jece.2016.11.034

[42] Kityk, A. A., Rublova, Y. D., Kelm, A., Malyshev, V. V., Bannyk, N. G., Flis-Kabulska, I. (2018). Kinetics and mechanism of corrosion of mild steel in new types of ionic liquids. *J. Electroanal. Chem*., *823*, 234–244. https://doi.org/10.1016/j.jelechem.2018.06.018

[43] Haerens, K., Matthijs, E., Binnemans, K., Van der Bruggen, B. (2009). Electrochemical decomposition of choline chloride based ionic liquid analogues. *Green Chem*., *11*, 1357–1365. https://doi.org/10.1039/b906318h

[44] Mares Badea, M. L., Cojocaru, A., Anicai, L. (2014). Electrode processes in ionic liquid solvents as mixtures of choline chloride with urea, ethylene glycol or malonic acid. *UPB Scientific Bulletin, Series B: Chemistry and Materials Science*, 76(3),. 21–32.

[45] Abbott, A. P., El Ttaib, K., Ryder, K. S., Smith, E. L. (2008). Electrodeposition of nickel using eutectic based ionic liquids. *Trans. Inst. Met. Finish*., *86*, 234–240. https://doi.org/10.1179/174591908X327581

[46] Ali, M. R., Rahman, M. Z., Saha, S. S. (2014). Electroless and electrolytic deposition of nickel from deep eutectic solvents based on choline chloride. *Ind. J. Chem. Technol*., *21*, 127–133.

[47] Protsenko, V.S., Makhota, D.O., Butyrina, T.E., Korniy, S.A., Danilov, F. I. (2024). Anodic surface treatment of nickel in eutectic ionic liquids based on

choline chloride for electrochemical polishing and enhancement of electrocatalytic activity in hydrogen evolution reaction. *Voprosy Khimii i Khimicheskoi Tekhnologii*, (1), 89–98. https://doi.org/10.32434/0321-4095-2024-152-1-89-98

[48] Oriňáková, R., Turoňová, A., Kladeková, D., Gálová, M., Smith, R. M. (2006). Recent developments in the electrodeposition of nickel and some nickel-based alloys. *J. Appl. Electrochem*., *36*, 957–972. https://doi.org/10.1007/s10800-006-9162-7

[49] Lyons, M. E. G., Brandon, M. P. (2008). The oxygen evolution reaction on passive oxide covered transition metal electrodes in aqueous alkaline solution. Part 1 – nickel. *Int. J. Electrochem. Sci*., *3*, 1386–1424.

[50] Vedharathinam, V., Botte, G. G. (2013). Direct evidence of the mechanism for the electro-oxidation of urea on $Ni(OH)_2$ catalyst in alkaline medium. *Electrochim. Acta*, 108, 660–665. https://doi.org/10.1016/j.electacta.2013.06.137

[51] Protsenko, V. S., Makhota, D. O., Korniy, S. A., Butyrina, T. E., Danilov, F. I. (2024). Influence of anodic treatment of nickel in deep eutectic solvents on electrocatalytic activity in oxygen evolution and urea oxidation reactions. *Voprosy Khimii i Khimicheskoi Tekhnologii*, (3), 145–154. http://dx.doi.org/10.32434/0321-4095-2024-154-3-145-154

[52] Munde, A. V., Mulik, B. B., Dighole, R. P., Sathe, B. R. (2021). Urea electro-oxidation catalyzed by an efficient and highly stable Ni–Bi bimetallic nanoparticles. *ACS Appl. Energy Mater*., *4*, 13172–13182. https://doi.org/10.1021/acsaem.1c02755

[53] Zhang, J., Zhu, J., Kang, L., Zhang, Q., Liu, L., Guo, F., Li, K., Feng, J., Xia, L., Lv, L., Zong, W., Shearing, P. R., Brett, D. J. L., Parkin, I. P., Song, X., Mai, L., He, G. (2023). Balancing dynamic evolution of active sites for urea oxidation in practical scenarios. *Energy Environ. Sci*., *16*, 6015–6025. https://doi.org/10.1039/d3ee03258b